

A CHARACTERIZATION OF THE INTERFACIAL AND INTERLAMINAR  
PROPERTIES OF CARBON NANOTUBE MODIFIED CARBON  
FIBER/EPOXY COMPOSITES

A Thesis

by

RYAN SAGER

Submitted to the Office of Graduate Studies of  
Texas A&M University  
in partial fulfillment of the requirements for the degree of  
MASTER OF SCIENCE

May 2008

Major Subject: Aerospace Engineering

A CHARACTERIZATION OF THE INTERFACIAL AND INTERLAMINAR  
PROPERTIES OF CARBON NANOTUBE MODIFIED CARBON  
FIBER/EPOXY COMPOSITES

A Thesis

by

RYAN SAGER

Submitted to the Office of Graduate Studies of  
Texas A&M University  
in partial fulfillment of the requirements for the degree of

MASTER OF SCIENCE

Approved by:

Chair of Committee,	Dimitris C. Lagoudas
Committee Members,	Yongmei Jin
	Zoubeida Ounaies
Head of Department,	Helen Reed

May 2008

Major Subject: Aerospace Engineering

## ABSTRACT

A Characterization of the Interfacial and Interlaminar Properties of Carbon Nanotube Modified Carbon Fiber/Epoxy Composites. (May 2008)

Ryan Sager, B.S., Texas A&M University

Chair of Advisory Committee: Dr. Dimitris C. Lagoudas

The mechanical characterization of the interfacial shear strength (IFSS) of carbon nanotube (CNT) coated carbon fibers and the interlaminar fracture toughness of woven fabric carbon fiber/epoxy composites toughened with CNT/epoxy interleave films is presented. The deposition of multiwalled carbon nanotubes (MWCNT) onto the surface of carbon fibers through thermal chemical vapor deposition (CVD) was used in an effort to produce a graded, multifunctional interphase region used to improve the interfacial strength between the matrix and the reinforcing fiber. Characterization of the IFSS was performed using the single-fiber fragmentation test. It is shown that the application of a MWCNT coating improves the interfacial shear strength between the coated fiber and matrix when compared with un-coated fibers. The effect of CNT/epoxy thin interleave films on the Mode I interlaminar fracture toughness of woven fabric carbon/epoxy composites is examined using the double-cantilever beam (DCB) test. Initiation fracture toughness, represented by critical strain energy release rate ( $G_{IC}$ ), is shown to improve over standard un-toughened composites using amine-functionalized CNT/epoxy thin films. Propagation fracture toughness is shown to remain unaffected using amine-functionalized CNT/epoxy thin films with respect to standard un-toughened composites.

To my wife, who has always believed in me

## ACKNOWLEDGMENTS

I wish to express my sincere gratitude to Dr. Dimitris Lagoudas, Dr. Yongmei Jin and Dr. Zoubeida Ounaies, my advisory committee, for their guidance and support. I also wish to thank Patrick Klein for his patience, guidance and support during my graduate career. Finally, I wish to thank all of my collaborators, especially Dr. Jeffery Baur at the Air Force Research Laboratory and Qihong Zhang at the University of Dayton along with the entire staff at AFRL Materials and Manufacturing Directorate. Funding for this research provided by Air Force Research Laboratory, Minority Leaders Program, F33601-05-D-1912

## TABLE OF CONTENTS

CHAPTER	Page
I	INTRODUCTION . . . . . 1
II	MECHANICAL AND INTERFACIAL STRENGTHS OF CNT COATED CARBON FIBERS . . . . . 4
	A. Experimental . . . . . 7
	1. Specimen materials . . . . . 7
	2. Surface treatments . . . . . 8
	3. Single-fiber tensile testing . . . . . 9
	4. Single-fiber fragmentation testing . . . . . 10
	5. Specimen fabrication . . . . . 12
	6. Test procedure . . . . . 12
	B. Results . . . . . 15
	1. Fiber tensile results . . . . . 15
	2. Fragmentation results . . . . . 16
	C. Conclusions . . . . . 22
III	EFFECT OF CARBON NANOTUBE/EPOXY INTERLEAF FILMS ON THE INTERLAMINAR FRACTURE TOUGH- NESS OF WOVEN FABRIC CARBON/EPOXY COMPOSITES 24
	A. Experimental Setup . . . . . 26
	B. Experimental Procedure . . . . . 30
	C. Results . . . . . 32
	D. Conclusions . . . . . 39
IV	OVERALL CONCLUSIONS AND FUTURE WORK . . . . . 40
	REFERENCES . . . . . 43
	VITA . . . . . 49

## LIST OF TABLES

TABLE		Page
I	Measured physical and mechanical properties of single fiber specimens.	17
II	Fragmentation test results for various fiber types. . . . .	19
III	Fiber and matrix properties. . . . .	27
IV	Interleave film properties. . . . .	27
V	Initiation fracture toughness values. . . . .	35
VI	Propagation fracture toughness values. . . . .	36

## LIST OF FIGURES

FIGURE	Page
1	High resolution SEM images of a) carbon fiber with randomly oriented MWCNTs b) carbon fiber with radially aligned MWCNTs. . . . . 9
2	Schematic of saturated specimen. . . . . 11
3	a) Fragmentation test fixture b) Test fixture under microscope. . . . . 14
4	Weibull plots of tensile strength data for various fiber surface treatments. 18
5	Plot of number of fragments/mm vs. composite stress for each fiber type tested. . . . . 20
6	Birefringence effects of fragmented specimens at 10x magnification. . . . . 21
7	Schematic of PAMAM-0 . . . . . 28
8	Schematic of heated VARTM lay-up. . . . . 29
9	DCB specimen after testing. . . . . 31
10	Representative load-displacement curves for DCB specimens. . . . . 33
11	Representative <i>R</i> -curves for DCB specimens: (a) Standard panels; (b) Neat and As-received XD CNT panels; (c) Amino-functionalized XD CNT panels. . . . . 34
12	Representative failure surfaces for various panels: a) Standard panels; b) Neat epoxy interleaved panel; c) As-received XD CNT/epoxy interleaved panel; d) Amino-functionalized XD CNT/epoxy interleaved panel 1; e) Amino-functionalized XD CNT/epoxy interleaved panel 2. . . . . 37
13	Propagation fracture toughness values for functionalized panels 1 & 2. . . . . 38



## CHAPTER I

### INTRODUCTION

Fiber reinforced composites have been used commercially for decades, specifically with fiber reinforced polymer composites (FRPC) becoming more common, especially within the aerospace, automotive and recreational sports industries. Generally, strong fabric layers or unidirectional fiber tapes are layered in a specific sequence and bonded together by a matrix material to provide a strong and light weight composite laminate whose mechanical properties are optimized for a specific loading configuration. While laminates are usually optimized to provide a mechanical solution to a specific loading along the fiber plane, often the out-of-plane mechanical, thermal or electrical properties are left in a less than optimal configuration. Within FRPCs, there exist many limiting factors, including a susceptibility to out-of-plane damage. The reinforcing fiber is generally a carbon or glass fiber while the polymer matrix is usually a brittle epoxy system. The brittle nature of epoxy systems can limit the matrix toughness, often resulting in matrix cracking. Additionally, weak interfaces can lead to fiber-matrix interfacial failure and delamination. Finally, epoxy is electrically and thermally insulating, producing a large discrepancy between in-plane and out-of-plane conductivities.

Multifunctional materials, or materials which possess both optimized mechanical and thermal properties or mechanical and electrical properties, have been sought by researchers and industry as a way to utilize the same bulk material for multiple uses. While carbon fiber reinforced polymer composites offer excellent in-plane mechanical properties as well as good in-plane thermal and electrical conductivity, the poor out-

of-plane properties leave much to be desired. An improvement in the transverse conductivities of composite laminates could lead to in-situ damage sensing, improved thermal dissipation, lightning strike dissipation as well as a host of other benefits. Similarly an improvement in the mechanical properties in the transverse direction, such as improved matrix toughness and improved fiber-matrix interfacial strength, would reduce the susceptibility of composite laminates to out-of-plane damage as well as improve the overall efficiency of the composite.

With their small size and exceptional mechanical, electrical and thermal properties, carbon nanotubes (CNT) are unique materials which have come to the forefront of today's materials research. Their exceptional strength, stiffness and failure strain make them attractive reinforcement materials, while their characteristic electrical response to load make them ideal candidates for use as sensors and actuators [1–7]. Their high thermal conductivity provides an opportunity for thermal management applications as well [8, 9]. By incorporating CNTs into traditional composites, there exists a possibility to produce multifunctional composites. Veedu et al. [10] have demonstrated this by measuring improvements in multiple mechanical and nonmechanical properties including interlaminar fracture toughness and transverse thermal and electrical conductivity of silicon carbide fiber reinforced epoxy composites with the addition of carbon nanotube “forests”. While impressive, a significant amount of composites use carbon fiber as a reinforcing material instead of silicon carbide due to carbon fiber's lower density and higher strength. It is here that an attempt is made to produce multifunctional carbon fiber reinforced nanocomposites using two separate methods to disperse multi-walled carbon nanotubes (MWCNTs) within traditional carbon fiber reinforced polymer composites.

Due to the cost associated with the use of CNTs within traditional FRPCs, it is desirable to process the composite in such a way that the most beneficial attributes

of the CNTs are utilized while minimizing the amount of material used. To achieve this, novel methods of CNT placement and dispersion within the bulk composite are needed which allow for easy processibility as well as direct control of CNT location and orientation. In the following chapters, two methods for placing multi-walled carbon nanotubes into traditional fiber reinforced polymer composites will be examined. The first method will utilize chemical vapor deposition (CVD) as a method for directly growing MWCNTs on a carbon fiber substrate. The benefit in using this method is that the location and orientation of the grown CNTs can be easily controlled. Additionally, the local volume fraction of CNTs near the fiber surface can reach close to 50%, a value much higher than can be achieved through traditional mixing techniques [11]. In this method, a tow of carbon fiber consisting of 6000 carbon fiber filaments is coated with MWCNTs using CVD. Individual filaments are then removed from the tow and tested to determine both the mechanical properties as well as the interfacial strength of the coated fibers within an epoxy matrix. The CVD method for depositing nanotubes onto a carbon fabric substrate could then be used to produce entire CNT coated carbon fabric plies for use in fiber reinforced polymer composite laminates. These laminates would be produced through the vacuum assisted resin transfer moulding (VARTM) method of matrix infusion however this composite fabrication is not presented here. The second method of introducing CNTs examined in this study will utilize a thin MWCNT/epoxy nanocomposite interleaf film which is easily incorporated within a standard composite laminate. The MWCNTs are first dispersed within a bulk epoxy and then fabricated into a thin b-staged interleaf film. This interleaf film is then easily incorporated into standard composite laminates produced using the VARTM method. The effect of MWCNT/epoxy interleaf films on the Mode I fracture toughness of carbon fabric/epoxy composite laminates will be investigated.

## CHAPTER II

MECHANICAL AND INTERFACIAL STRENGTHS OF CNT COATED  
CARBON FIBERS

With their small size and exceptional mechanical, electrical and thermal properties, carbon nanotubes (CNT) are unique materials which have come to the forefront of today's materials research. Their exceptional strength, stiffness and failure strain make them attractive reinforcement materials, while their characteristic electrical response to load make them ideal candidates for use as sensors and actuators [1–7]. Their high thermal conductivity provides an opportunity for thermal management applications as well [8, 9]. By utilizing one or more of these characteristics along with other materials, truly multifunctional composites could be produced.

Carbon nanotubes are essentially graphene sheets in the shape of a tube whose diameter is on the order of nanometers [12]. Various morphologies exist, including armchair and zigzag which define the orientation of the lattice with the tube axis (chirality). Other variations such as double walled and multiwalled carbon nanotubes (MWCNT) exist, which are defined by two or more nested SWCNTs. Carbon nanotubes are commonly produced through three types of processes: carbon-arc discharge, laser ablation of carbon, and chemical vapor deposition (CVD) [13]. While all three methods are used to produce bulk amounts of CNTs, only chemical vapor deposition provides a method to produce CNTs which are grown directly onto reinforcing fibers, which can then be used in traditional fiber-reinforced polymer composites (FRPC). The CVD process provides direct control of location, alignment, morphology and packing density of CNTs while providing strong bonds with a substrate [14]. For FRPCs, this eliminates problems associated with dispersion of CNTs within a matrix material as well as problems of orienting them within a matrix material. Di-

rect growth of CNTs on reinforcing fibers therefore promises to be a useful method of producing multifunctional nanocomposites where control of dispersion, alignment, length and morphology of CNTs within a composite is desired.

The mechanical behavior of composites depend not only on the properties of the constituent materials, but on the characteristics of the interface(s) between the constituents as well. In continuous fiber reinforced composites, the load is transferred from the matrix to the fiber through shear. With poor interfacial strength, less shear stress is capable of being transferred to the fiber, creating a weaker, less efficient composite. The interfacial strength can be improved through various methods, the most common being through improving the chemical adhesion of the fiber with the matrix, removing the weak outer layer of the fiber produced during fiber fabrication, or by producing an interphase region through the use of a thin polymer sizing [15, 16]. The application of a surface treatment during initial processing is useful in applying a surface chemical group to enhance the interaction of the fiber surface with the matrix. Additionally, the surface treatment is also effective at removing a weak outer surface layer [15]. Drzal et al. showed that the most effective result of applying a surface treatment is the removal of the weak outer layer produced during fiber fabrication. The application of a thin polymer coating, referred to as sizing, is useful in producing an interphase region which has material properties different than the surrounding bulk matrix. Typically, in epoxy sizings, a higher elastic modulus and lower fracture toughness interphase region is produced by non-stoichiometric chemistry. This results in increasing the shear stress transfer to the fiber while providing an alternative for cracking to proceed into the matrix as opposed to failing the fiber interface [16, 17]. While not seen by Drzal et al., the thin polymer sizing may also provide a protective function for the fiber surface during handling.

CNT coated fibers have the potential to increase composite mechanical properties

while providing for additional electrical or thermal multifunctionality; however the primary role of fiber-reinforced composites is still structural. As such, it is important to ensure that the structural performance of the composite is maintained or improved along with the improvement in multifunctionality. This study focuses on the effect of CVD applied CNTs on the mechanical properties of carbon fiber-reinforced epoxy composites.

Thostenson et al. [18], have previously demonstrated an improvement in interfacial shear strength of carbon fibers coated with MWCNTs. However, in their paper they assumed the strength of the fibers would not be affected during the CVD process even though the processing temperatures associated with the growth of CNTs studied in their paper exceeded 650°C. It has been shown that the high temperatures and reactive conditions used during CNT processing can significantly degrade the mechanical properties of carbon fiber. In fact, degradation of mechanical properties of carbon fiber can occur when subjected to oxygen at temperatures as low as 400°C [19]. By assuming a constant strength between as-received fibers and fibers which had been subjected to CVD processing, the interfacial strength of the processed fibers could be overestimated using the standard Kelly-Tyson [20] method of calculating interfacial shear strength. Additionally, only one orientation of CNTs, appearing to be randomly oriented, was studied by Thostenson. With the ability to control the orientation of the CNTs with respect to the fiber axis, an examination into the effect of CNT orientation is possible.

In this study, T650 carbon fibers are coated with multi-walled carbon nanotubes through the use of thermal chemical vapor deposition in both a random and radially aligned morphology. The fiber tensile strength and modulus of CNT coated fibers are then examined using the single-fiber tensile test. These results are then compared to those of untreated sized and unsized T650 carbon fibers in an effort to determine

to what degree the fiber mechanical properties are degraded due to thermal CVD growth of CNTs. Additionally, the effect of the presence as well as the orientation of CNTs on the interfacial shear strength of CNT coated carbon fibers is studied using the single-fiber fragmentation test. The interfacial shear strength is calculated using the Kelly-Tyson method.

### A. Experimental

A series of single-fiber tensile tests were initially performed on fibers with each type of fiber treatment to determine the effect each treatment had on the axial properties of the fibers. Once the tensile data was compiled, a series of single-fiber fragmentation tests were performed in order to determine the effect of the treatments on the interfacial shear strength between the fiber and the epoxy matrix.

#### 1. Specimen materials

The resin used in this study was EPIKOTE 862 resin (Hexion Specialty Chemicals, Inc.) with EPIKURE Curing Agent W (Hexion Specialty Chemicals, Inc.). EPIKOTE 862 is a bisphenol-F epoxy resin with an aromatic amine. Resin was mixed with the curing agent at 100 : 26.4 by weight. Curing temperature and procedure were 2 hours at 121°C followed by 2 hours at 177°C. EPIKOTE 862/W was used in this test due to its high strain to failure, its transparency, and its ability to adhere well to carbon fiber reinforcement.

The carbon fibers used in this study were Thornel T650 (Cytec Industries), a high modulus polyacrylonitrile (PAN) based fiber used extensively within the aerospace industry with high strength and low strain to failure. It is commercially available in two variants, sized and unsized. The sized fibers are coated with a thin (typically

1wt.%) epoxy surface coating which is specifically formulated to adhere well with an epoxy matrix, as well as improve handling and decrease damage during processing and handling. The unsized fibers do not have this surface coating. Neither fiber type was subjected to an oxidative surface treatment. Once received, various samples of the unsized fibers were further treated through CVD processing in which MWCNTs were grown on the fiber surface.

## 2. Surface treatments

Two CVD treatments were used; one produced MWCNTs which were radially aligned with respect to the fiber surface, and another which produced randomly oriented MWCNTs with respect to the fiber surface. Growth conditions for the radially aligned MWCNTs included a pretreatment of the fiber surface with  $MgSO_4$  in alcohol followed by exposure to Iron Phthalocyanine  $Fe(CO)_5$  powder at  $900^\circ\text{C}$  for 15 minutes in an  $Ar/H_2$  environment. In this configuration, iron is used as the catalyst while the phthalocyanine is used as the carbon source. Growth conditions for the randomly oriented MWCNTs included a pretreatment of the fiber surface with  $MgSO_4$  in alcohol followed by exposure to a carbon source of xylene and a catalyst of ferrocene at  $800^\circ\text{C}$  for 30 minutes in an  $Ar/H_2$  environment. High resolution SEM images were taken of both morphologies to verify orientation and coverage, which can be seen in Fig. 1.



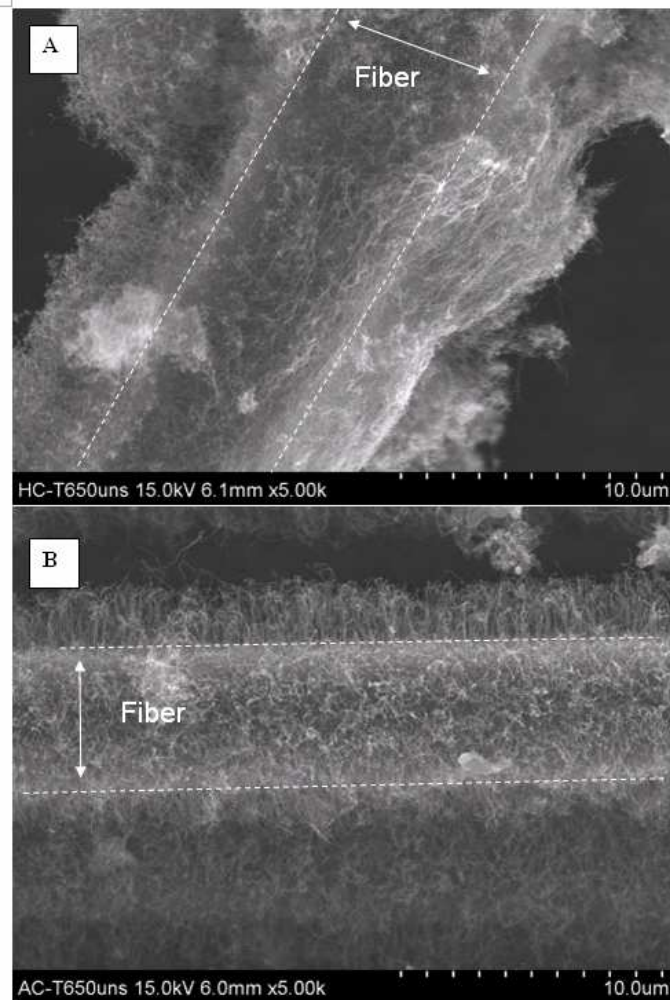


Fig. 1. High resolution SEM images of a) carbon fiber with randomly oriented MWCNTs b) carbon fiber with radially aligned MWCNTs.

### 3. Single-fiber tensile testing

A series of tests were performed in which a single fiber is subjected to tensile loading in accordance with ASTM D 3379-75. Force and displacement measurements are taken which are then used to determine the ultimate tensile strength and axial modulus of the specimen. Tests were performed on each fiber type in order to determine the

effect each surface treatment had on the axial properties. Individual fiber diameters were measured using an optical microscope equipped with a Vickers- A.E.I. Image Splitting Eyepiece. Tensile testing was performed on a Sintech 3365 5kN material test machine at a rate of 0.05in/sec. Data was collected at a rate of 5pts/sec.

#### 4. Single-fiber fragmentation testing

The single fiber fragmentation test (SFFT) has been commonly used within the literature to analyze the interfacial shear strength of a fiber embedded within a matrix [15, 16, 18, 21–28]. In this test, a single fiber is embedded axially within a dogbone shaped matrix specimen and subjected to a tensile load. The tensile load is transferred from the matrix to the fiber through shear stress at the interface, causing the fiber to elongate. As the fiber elongates, it begins to fragment, failing at its weakest points. Continued elongation results in continued fragmentation, until all the fragments are too short to transfer enough load to create sufficient tensile stress to break the fiber. By assuming a constant shear stress, the interfacial shear strength can be determined through a simple force balance equation of the fragment:

$$\tau = \frac{\sigma_f}{2} \left( \frac{d}{l_c} \right) \quad (2.1)$$

where  $\tau$  is the interfacial shear strength,  $\sigma_f$  is the ultimate fiber strength at the critical length,  $d$  is the fiber diameter, and  $l_c$  is the fiber critical length. Because a fiber will fragment whenever its length is greater than the critical length, a range of fragment lengths between  $l_c$  and  $l_c/2$  will be present upon saturation (Fig. 2). Assuming a normal distribution, the critical length  $l_c$  of a fiber can be determined using the measured average fragment length  $\bar{l}$  through the equation [28]:

$$l_c = \frac{4}{3} \bar{l} \quad (2.2)$$

where

$$\bar{l} = \frac{1}{N} \sum_{i=1}^N l_i \quad (2.3)$$

with  $l_i$ , the individual fragment lengths and  $N$ , the number of fragments within the gauge length. Therefore, when comparing two fibers of equal strength and diameter, the fiber with the shortest critical length will have the highest interfacial shear strength.

The test is performed under a light microscope so that fragmentation could be observed in-situ. Polarization is also used to view photoelastic effects such as birefringence caused by debonding of the interface as well as fiber fracture. Under polarization, the epoxy matrix is optically isotropic, but becomes anisotropic when subjected to stress [26]. The presence of bright birefringence at the points of fiber fracture is used here as a method to easily determine the fragment lengths during testing.

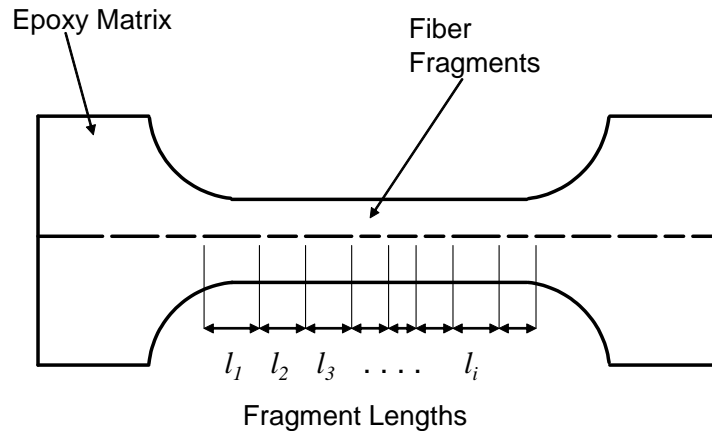


Fig. 2. Schematic of saturated specimen.

## 5. Specimen fabrication

Standard one dogbone molds with a 1in gauge length designed using a metal template. Molds were cast using a silicone rubber compound, GE Silicones RTV664A-1GP, mixed with a curing agent, GE Silicones RTV664B-01P, at a ratio of 10 : 1. The mold was then degassed for 3 hours under vacuum to remove any air bubbles and to ensure a smooth specimen surface. The molds were then allowed to cure at room temperature overnight. Post cure processing at elevated temperatures of 200°C for 2 hours was also performed to ensure that any remaining gasses would evacuate the mold and not disturb the epoxy dogbone specimens during processing.

Once the molds had been prepared, single fibers were placed axially within notches in the molds. Epoxy, which had been prepared and degassed, was then poured into the molds, taking special care to keep the fibers from moving to either side or in the through thickness direction. The specimens were then placed within an oven and cured for 2 hours at 121°C and then for 2 more hours at 177°C. After the specimens had cooled, they were removed from the molds and prepared for testing. Preparation included sanding down the uneven top of the resin with 600 and 1000 grit sandpaper to an even height of approximately 1.65mm. The surfaces of the specimens were then polished with 0.5 $\mu$ m alumina polishing solution until the embedded fiber could clearly be seen and no surface scratches were visible.

## 6. Test procedure

After the specimens have been adequately prepared, they are secured in the test apparatus and subjected to tensile load (Fig. 3a). The entire loading frame is placed under an optical microscope (Nikon Microphot-FXL) equipped with polarizers so that the fragmentation process can be observed insitu (Fig. 3b). Load is applied through

the use of a hand screw which pulls a chain upward. This pulling of the chain is translated into a tensile load along the axial direction of the dogbone specimen. A strain gauge is mounted to the test apparatus where the chain meets the specimen holder. The strain gauge is connected to a strain box and was calibrated to display the load applied. Load was originally applied to 60lbs and then held for a short time so that fragmentation could be observed. Once the number of fragments was counted, load was then applied in 5lb intervals, stopping with each to observe fragmentation and record images. Fragmentation initiation for all specimens occurred between 70lbs and 115lbs, with the majority initiating around 85lbs. Sized fibers initiated fragmentation at an average of 103lbs. Loading of the specimens continued until fragmentation of the fibers ceased or the specimen failed.

Fragmentation of the fiber was observed in-situ using polarized light. The use of polarizers allowed for the observance of birefringence within the epoxy matrix. As the fibers break and the interface fails, bright colorful patterns emerged around the fiber-matrix interface. This birefringence effect is a useful tool for observing stress patterns as well as observing the fracture of the opaque carbon fibers. As load is transferred to the fiber, stress will build along the fiber, creating a birefringent effect. When the fiber breaks, the stress drops to zero in the break gap between fiber fragments, producing an area of no birefringence. The observance of birefringent peaks separated by areas of no birefringence can be utilized to denote fiber breaks. Because both the fiber break gaps and the fibers themselves are dark under plain light, breaks within the fiber are difficult to observe. The use of birefringence however, gives the observer a useful tool for easily determining the existence of a fiber break. During testing, fiber fragments were counted using the observance of birefringence gaps while the specimen was under load.

After the number of fragments was counted for each loading increment, load

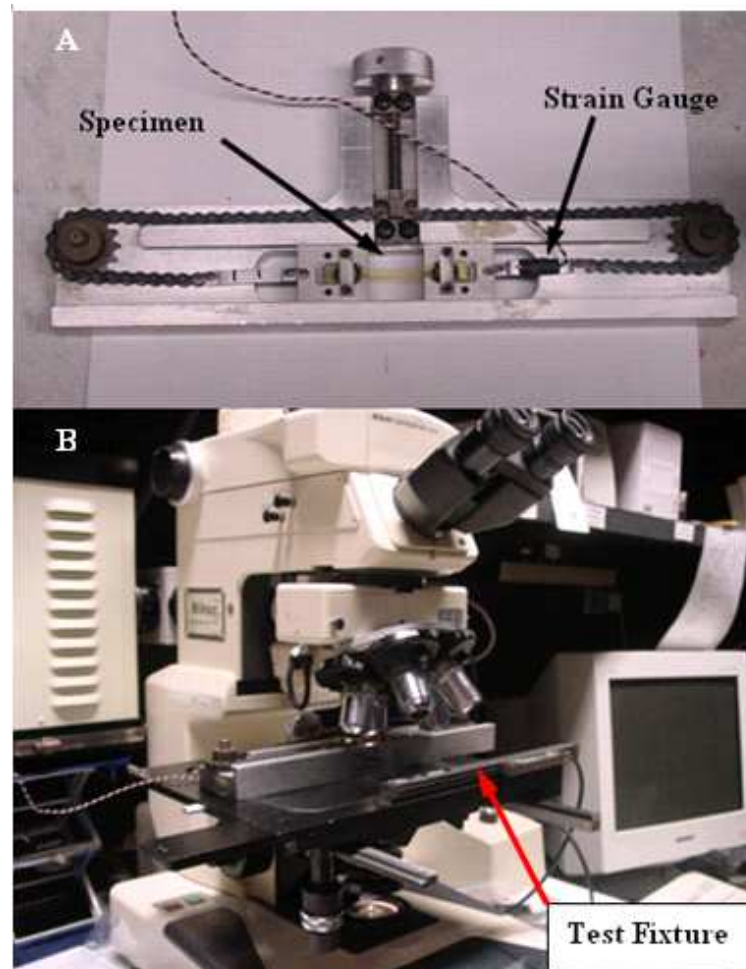


Fig. 3. a) Fragmentation test fixture b) Test fixture under microscope.

was then applied and the process was repeated. Average fragment length was then determined by dividing the number of fragments at the current load by the gauge length over which the observations were made. Once the fibers ceased to fragment with increasing load, the specimen was said to be saturated and the average fragment length was noted. Some specimens failed before a saturation state was achieved. In these cases, the final fragment length was not considered to be the saturation length and therefore the data was not used in shear strength calculations. The exception to

this however, was in the cases of sized fiber specimens. Throughout testing, none of the sized fiber specimens reached a critical length before the epoxy specimen failed. This was due to the increased strain to failure of the sized T650 fibers as compared to the other fibers tested. Because no saturation state was achieved for the sized fibers, the final fragment lengths were taken instead, resulting in an upper bound estimation for the fiber's critical length.

## B. Results

### 1. Fiber tensile results

The fiber tensile results, which can be seen in Fig. I, clearly demonstrate the effect on which surface treatment plays a role in tensile properties of fibers. Tests revealed a range in ultimate strengths and moduli both within fiber types as well as between fiber types. Sized T650 fibers were measured to have the highest tensile modulus and strength out of all types measured, with modulus and strength values of 217 and 4.02GPa respectively. As received unsized T650 fibers demonstrated lower modulus and strength values of 200 and 2.86GPa, respectively, a decrease of 8% in modulus and 29% in ultimate strength as compared to its sized counterpart. These decreases, especially in ultimate strength, are probably due to flaws introduced during the bundling and weaving process as well as during the removal of individual filaments from tows for testing combined with the lack of protection offered by a sizing.

Both nanotube coating processes significantly decreased the tensile strength of the carbon fiber. The ultimate strength of the randomly oriented CNT coated fibers decreased 30% from the as-received unsized values to an average strength of 1.99GPa. The modulus also decreased by 13% to a value of 175GPa. The ultimate strength of the aligned CNT coated fibers decreased 37% from the as-received unsized values to an

average strength of 1.79GPa. The modulus decreased by 9%. The decreases in fiber properties are most likely due to the presence of trace amounts of oxygen remaining within the CVD chamber. Subsequent optimization of the growth conditions has lead to unsized fibers coated with MWCNTs maintaining close to their original mechanical properties [11]. However, these were unavailable at the time of this testing.

It is widely observed that typical reinforcement fibers, including carbon, exhibit a size effect whereby shorter fibers give higher tensile strength measurements. This is due to the presence of flaws in the fiber from the manufacturing process, handling, and environmental effects. Longer fibers will have a greater amount, and likely more severe defects; therefore, the gauge length will affect the measured tensile properties of carbon fibers. A Weibull distribution often emerges as a good representation of fiber strength distribution, and can be used to estimate the length scale effect on tensile properties [29]. Weibull plots for each fiber type were produced using a two-dimensional Weibull statistical method. The statistical probability quantities  $Y=\ln(-\ln(1-P))$  were plotted versus the logarithm of fiber strength  $\sigma_{UTS}$  to produce a linear plot ("Weibull plot"), the slope of which is the Weibull shape parameter  $\rho$ . The value  $P$  is the cumulative probability distribution of the observed fiber strengths. The Weibull plots can be seen in Fig. 4. For all fiber types tested, few outliers were observed. The resulting shape parameters for each fiber type are shown in Fig. I.

## 2. Fragmentation results

Calculation of interfacial shear strengths were carried out for each specimen which reached a saturation state using equations for the shear strength  $\tau$  and the critical length  $l_c$  as described previously. The average fragment length for each specimen that reached a saturation state was used to calculate that specimen's critical length  $l_c$ . For each specimen's calculated critical length, the fibers ultimate tensile strength at the



Table I. Measured physical and mechanical properties of single fiber specimens.

Fiber Type	Diameter ( $\mu m$ )	Modulus ( $GPa$ )	$\sigma_{UTS}$ ( $GPa$ )	$\epsilon$ (%)	Weibull Shape Parameter	No. of Samples
Unsize Fiber	7.3	200	2.86	1.43	5.21	55
Sized Fiber	7.3	217	4.02	1.86	4.32	49
Unsize w/ Aligned CNT	7.2	182	1.79	0.99	4.02	56
Unsize w/ Random CNT	6.5	175	1.99	1.13	4.27	62

critical length was calculated using a simple weakest-link scaling function [29]:

$$\sigma_f = \sigma_{UTS} \left( \frac{l_c}{l_0} \right)^{\frac{-1}{\rho}} \quad (2.4)$$

where  $\sigma_f$  is the mean fiber tensile strength at the critical length,  $\sigma_{UTS}$  is the measured mean fiber tensile strength from tensile tests,  $l_c$  is the fiber critical length calculated in Equation 2.2,  $l_0$  is the fiber length used in the tensile tests, and  $\rho$  is the Weibull shape parameter measured from the tensile test results. The interfacial shear strength  $\tau$  was then calculated using the fiber tensile strength at the critical length, along with the critical length value. Interfacial strength results for each fiber type can be seen in Fig. II.

Tests revealed a large range in critical lengths as well as in calculated interfacial shear strength values, especially within the MWCNT coated fiber types. Both of the as-received fiber types performed consistently between their respective specimens in terms of critical lengths. This can be expected due to a consistency in manufacturing processes and therefore a consistency in strength once the major surface flaws were eliminated in the initial few fragmentations. However, it should be noted that within this set of tests, not a single sized fiber specimen achieved a true saturation state

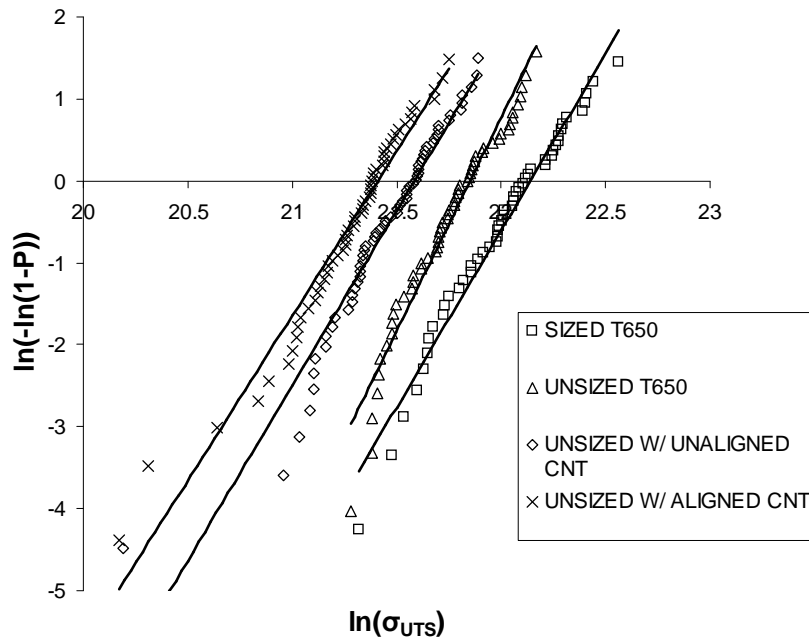


Fig. 4. Weibull plots of tensile strength data for various fiber surface treatments. The slopes of the linear curves denote the Weibull shape parameter for that surface treatment.

before specimen catastrophic failure. This can be seen in Fig. 5 by the lack of a plateau for the sized fiber specimens. For this reason, the average fragment length obtained immediately before specimen failure was used instead. This results in an upper bound for both the fiber critical length and thus a lower bound calculated interfacial shear strength.

The MWCNT coated fibers demonstrated a larger variation in their critical lengths and thus their calculated interfacial strength values. This variation indicates a non-uniformity of surface qualities among the fibers tested. One explanation of this is a discontinuous or inconsistent deposition of MWCNTs along fibers within the same bundle. Because the CVD process was performed on bundles of fibers, it

Table II. Fragmentation test results for various fiber types.

Fiber Type	$\sigma_{UTS}$ ( <i>GPa</i> )	Shape Parameter $\rho$	$\sigma_f$ ( <i>GPa</i> )	$l_c$ ( $\mu m$ )	$\tau_{KellyTyson}$ ( <i>MPa</i> )
Unsize Fiber	2.86	5.21	6.19	338	50.5
Sized Fiber	4.02	4.32	10.59	< 383	> 101.6
Unsize w/ Aligned CNT	1.79	4.02	5.19	362	56.2
Unsize w/ Random CNT	1.99	4.27	5.98	229	86.6

can be expected that variations in coverage will exist between fibers which were positioned near the outer surface of the fiber bundle as opposed to fibers which were positioned near the middle. Although a concerted effort was made to separate the individual fibers from the same area of the bundle, variations in coverage will still exist.

Calculations indicate that sized T650 has the strongest interfacial strength. This is probably due both to the excellent adhesion created between the fiber and the matrix as well as the non-stoichiometric interphase produced by the sizing. Drzal et al. demonstrated that the main effect of a sizing is to produce a brittle interphase region surrounding the fiber. The sizing usually contains less than a stoichiometric amount of curing agent, creating a layer having a higher modulus along with lower fracture toughness. The higher modulus increases the shear stress transfer to the fiber whereas the decreased fracture strength directs the failure away from the interface and into the matrix [16]. The effect of modulus on shear transfer has been validated using finite element modeling [17]. Fig. 6 demonstrates the photoelastic effects of the various fibers. It can clearly be seen that the birefringence along the sized fiber is relatively small indicating limited interfacial debonding. Large matrix cracking is

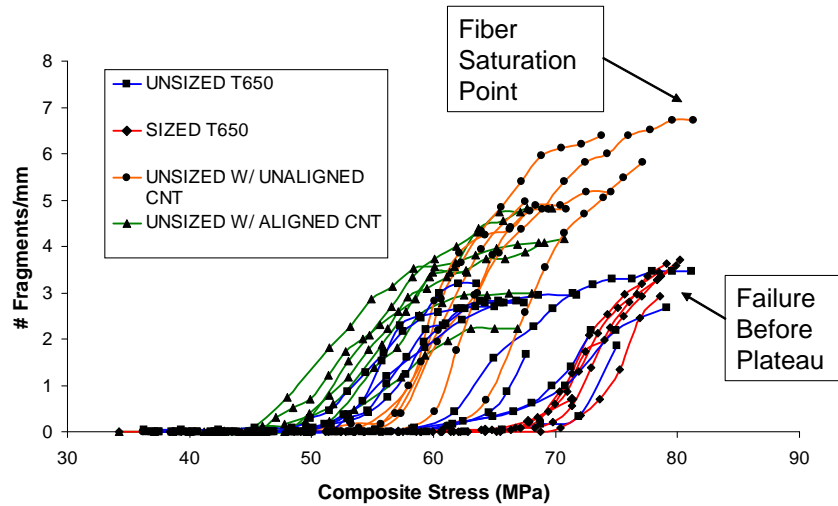


Fig. 5. Plot of number of fragments/mm vs. composite stress for each fiber type tested.

The fragment saturation point is determined when the number of fragments remains constant with increasing load. Variations in critical length within individual fiber types can clearly be seen.

also seen at the fiber break, indicative of the reduced fracture toughness interphase region created by the sizing.

The randomly oriented MWCNT coated fibers provided the next best interfacial shear strength, followed by aligned MWCNT coated fibers and finally the untreated fibers. Randomly oriented MWCNT and aligned MWCNT coated fibers demonstrated a 71% and 11% increase in calculated shear strength, respectively over that of the untreated fiber from which it was processed. This increase is most likely due to the presence of the nanotubes along the interface producing a strengthening effect. This can be seen in Fig. 6. The birefringence along the MWCNT coated fibers is small indicating limited interfacial failure and therefore good adhesion. The difference in interfacial shear strength observed between the aligned and randomly oriented MWCNT coated fibers is probably due to a strengthening effect of tubes oriented

along the loading direction within the randomly oriented specimens. Observations of the unsized fiber demonstrate a long, flat region of birefringence. This is indicative of a weak interface and corroborates the low interfacial shear strength values obtained from testing. These low values are most likely due to a weak bond between the fiber surface and the matrix.

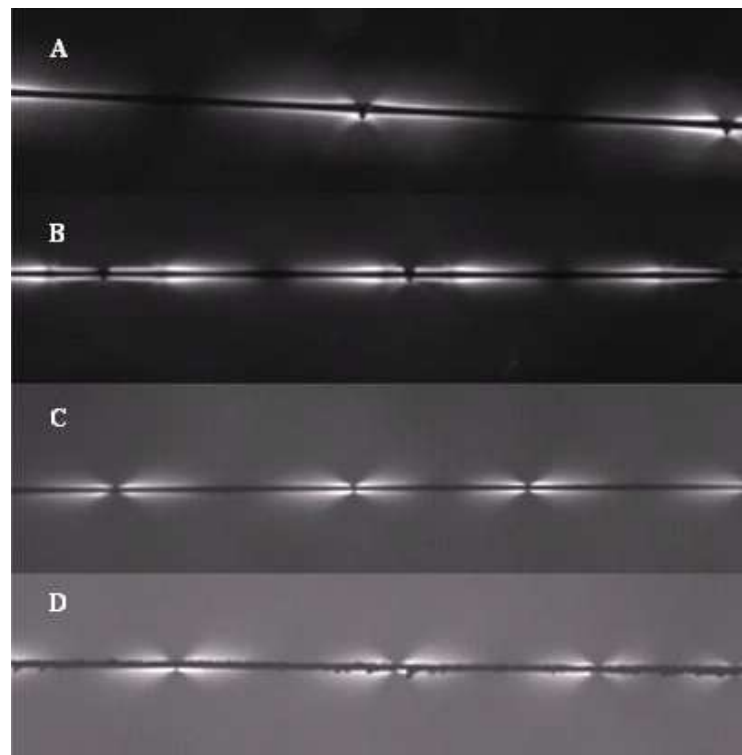


Fig. 6. Birefringence effects of fragmented specimens at 10x magnification. a) Sized T650 b) Unsized T650 c) Aligned CNT d) Random CNT.

### C. Conclusions

Tensile and single-fiber fragmentation tests were performed on single T650 carbon fibers which had been coated with multi-walled carbon nanotubes through chemical vapor deposition (CVD). Results were compared to commercially treated and unsized fibers in an effort to determine what effect MWCNTs have on the tensile and interfacial properties of a fiber embedded within a polymer matrix. Tensile tests revealed that CVD processing has a major effect on the mechanical properties of the fiber, decreasing the ultimate tensile strength of the fiber by an average of 37% in the case of the radially aligned MWCNTs and by 30% in the case of randomly oriented MWCNTs. Similarly, a slight reduction in the average tensile modulus of the fiber by 9% and 13% was observed in the radially aligned and randomly oriented MWCNT coated fibers, respectively. Reductions in mechanical properties of the fiber due to processing can be attributed to the addition of surface flaws to the fiber through thermal degradation and surface oxidation. Decreased processing temperatures as well as the elimination of oxygen within the processing chamber have been shown to decrease this degradation in mechanical properties [11].

Single fiber fragmentation tests were performed on each fiber type in an effort to determine the effect of surface treatment on interfacial shear strength. The Kelly-Tyson model was used to calculate interfacial shear strength based on a fiber's critical fragment length as well as its ultimate tensile strength at said length. Results indicated that commercially sized fibers have the highest interfacial shear strength. Randomly oriented MWCNT and aligned MWCNT coated fibers demonstrated a 71% and 11% increase in interfacial shear strength over untreated fibers. This can be attributed to an increase in the interfacial strength due to the presence of the nanotubes. The difference in shear strength values between the two MWCNT coated

fiber types is most likely due to reinforcement provided by nanotubes aligned in the loading direction.

## CHAPTER III

EFFECT OF CARBON NANOTUBE/EPOXY INTERLEAF FILMS ON THE  
INTERLAMINAR FRACTURE TOUGHNESS OF WOVEN FABRIC  
CARBON/EPOXY COMPOSITES

Woven fabric carbon/epoxy composites have been embraced by the aerospace, automotive, and sporting goods industry due to their high in-plane specific strength and stiffness. However, like other laminate materials, they are most vulnerable to out-of-plane loading, often failing in delamination. Efforts to improve the interlaminar strength of laminate composites have met with some success, including 3-D reinforcement and improvements in the toughness of the matrix through additives.

Through-thickness reinforcement through 3-D weaving and Z-pinning has shown promising gains in interlaminar toughness; however due to damage caused to the reinforcing fibers from the weaving process, as well as through the insertion of the Z-pins, in-plane properties are reduced [30]. Most successful attempts to improve the toughness of the matrix have focused on the addition of modifiers to the matrix such as thermoplastic resins, rubbers, and particles. However, the addition of thermoplastics and rubbers may result in significant degradation of the matrix properties, such as strength, stiffness and glass transition temperature [31].

Due to their high specific stiffness, strength, and electrical and thermal conductivity, along with their low density, small size, high surface area to volume ratio and high aspect ratio, carbon nanotubes (CNTs) can have a significant effect on the bulk material properties of resins even when mixed in low weight percents. This improvement includes greater resin toughness while still maintaining or even improving other basic properties, especially strength, stiffness, and electrical and thermal conductivity [32–34]. One of the greatest difficulties in using CNTs, however, is dis-



persing them effectively within a matrix. Due to their high surface area and large aspect ratios, CNTs have a strong tendency to agglomerate, resulting in poor dispersion throughout the matrix. Conventional methods of dispersion, such as sonication, are only effective on small batches of material due to the extreme reduction in vibrational energy with increasing distance from the sonic tip [32], thus making large scale mixing of nanotubes both difficult and time consuming. Surface modification, especially through functionalization, has led to improvements in the ability of raw CNTs to disperse throughout a matrix. The functionalization has also been shown to increase the interfacial bond between the CNTs and the matrix [34, 35]. The combination of good CNT-matrix adhesion, dispersion, and the entanglement effect of embedded nanotubes within the matrix have been attributed to increased fracture toughness values of the bulk material by up to 18% over neat epoxy with only 0.1wt.% amino-functionalized double-wall carbon nanotubes (DWCNT) and a 26% increase in fracture toughness using only 1.0wt.% functionalized DWCNTs [32]. Similarly, tensile strength and Young's Modulus were also improved with the addition of functionalized CNTs [32].

Although effective methods of dispersing CNTs into resins have been devised, the addition of CNTs to the resin, even in small weight fractions, can lead to dramatic increases in resin viscosity. This increased viscosity can make common composite infusion molding techniques such as Vacuum Assisted Resin Transfer Molding (VARTM) difficult or impractical. Therefore a procedure which combines the effective laminate processing techniques such as VARTM with effective CNT-resin mixing techniques is needed. To that end, thin adhesive interleave films have been shown to improve the interlaminar fracture toughness and impact resistance of laminate composites [36–38]. Interleave films are easily positioned and incorporated within a laminate composite using standard processing techniques. With the incorporation of CNTs

within a thin epoxy interleave film, there exists an opportunity to specifically place a well-dispersed, CNT toughened layer within a composite laminate. The placement of a well-dispersed CNT toughened layer will also serve as an opportunity to provide additional benefits in out-of-plane thermal and electrical conductivity.

In this research, we have investigated the Mode I interlaminar fracture behavior of woven carbon fiber-epoxy laminates that have been reinforced with CNTs by the incorporation of thin, b-staged CNT-epoxy nanocomposite interleaf films. Double cantilever beam (DCB) specimens are used for the measurement of  $G_{Ic}$ , the critical strain energy release rate (fracture toughness) and the generation of resistance curves. Post-fracture microscopic inspection of the fracture surfaces is performed to determine crack paths and crack morphology.

#### A. Experimental Setup

The laminates under investigation were fabricated using EPIKOTE 862 resin cross-linked with EPIKURE W curing agent, with twenty layers of Hexcel four-harness satin weave carbon fiber fabric (SGP203) with identical warp and fill yarns. The fabric is comprised of Hexcel IM7 carbon fiber, an intermediate modulus fiber commonly used in the aerospace industry, and have a  $6K$  yarn fiber count. The fiber and resin properties from the manufacturer’s data sheets are summarized in Table III [39, 40]. Balanced, symmetric laminates were laid up with the yarns aligned with the panel  $x$  and  $y$  directions. The stacking sequence has the direction of the yarns facing the panel mid-plane alternating between 0 and 90 degrees.

Panels were fabricated incorporating a single b-staged EPIKOTE 862/W interleaf film at the mid-plane, as well as four panels without any film referred here as “standard” panels. The b-staged interleaf films were fabricated in the Polymer Tech-

Table III. Fiber and matrix properties.

Property	Hexcel IM7	EPIKOTE 862/W
Density ( $g/cm^3$ )	1.79	1.2
Modulus ( $GPa$ )	276	2.72
Tensile Strength ( $MPa$ )	5480	78

nology Center at Texas A&M University. XD grade CNTs (Carbon Nanotechnologies, Inc.) were incorporated into bulk EPIKOTE 862/W to produce two separate XD CNT/epoxy mixtures. These mixtures included amino-functionalized and untreated (as-received) XD CNTs. Amine functionalization was performed using PAMAM-0 dendrimer. PAMAM-0 is a dendrimer with four surface groups and a molecular weight of 517. A schematic of PAMAM-0 can be seen in Fig. 7. Surface modification to the CNTs as well as their incorporation into the bulk resin to produce the CNT/epoxy mixtures followed the procedures outlined by Sun et al. [41]. Once the CNT/epoxy materials had been produced, thin epoxy interleaf films were fabricated using a modified Elcometer 4340 automatic film applicator. The thin films were then cured to a B-stage of 50%. All CNT modified films contained 0.5 weight percent XD grade CNTs and ranged in thickness from 28 – 137 $\mu m$ . An additional neat EPIKOTE 862/W interleaf film was also prepared for use as a control. Parameters for all films used can be seen in Table IV.

Table IV. Interleave film properties.

CNT Type and Wt. % CNT	$T_g$ ( $^{\circ}C$ )	Thickness ( $\mu m$ )	
Neat Epoxy	0	38.1	28
As-Received	0.5	45.6	43
Functionalized 1	0.5	36.2	122
Functionalized 2	0.5	36.2	137

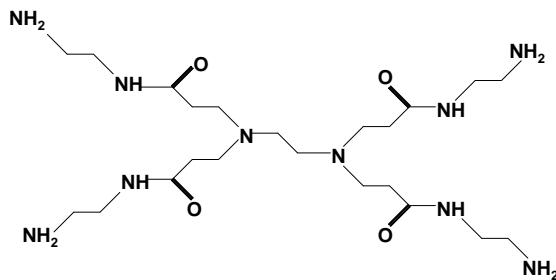


Fig. 7. Schematic of PAMAM-0.

The films were too fragile to handle without the backing paper, and therefore had to be thermally transferred to the lower of the middle fabric layers to place it into the lay-up. This was accomplished by laying the film on an aluminum plate face up with the fabric on top. A vacuum bag was then placed over the film and fabric, and vacuum applied while the aluminum plate was heated to between 15 and 20°C above the film  $T_g$ . The backing paper could then be peeled off, leaving the film intact, adhered to the fabric layer. This transfer process did not affect the  $T_g$  of the films.

The laminates were fabricated using a heated vacuum assisted resin transfer molding process (H-VARTM) developed by Bolick and Kelkar at North Carolina A&T University [42]. A schematic of the complete lay-up is shown in Fig. 8. Two vacuum bags, an inner bag and an outer bag, are used. The purpose of the outer bag is two-fold. First, it acts to constrain expansion of the inner bag during resin infusion, and then it acts as a fail-safe should the seal of the inner bag become compromised during the infusion process, or during subsequent curing. The reinforcement was laid up on a glass plate mold, which lies on top of temperature-controlled heating pads.

Vacuum is maintained on the inner bag for a minimum of twelve hours (overnight) to remove as much adsorbed air and water vapor as practical before resin infusion. Vacuum is then applied to the outer bag, and the bottom surface of the glass plate

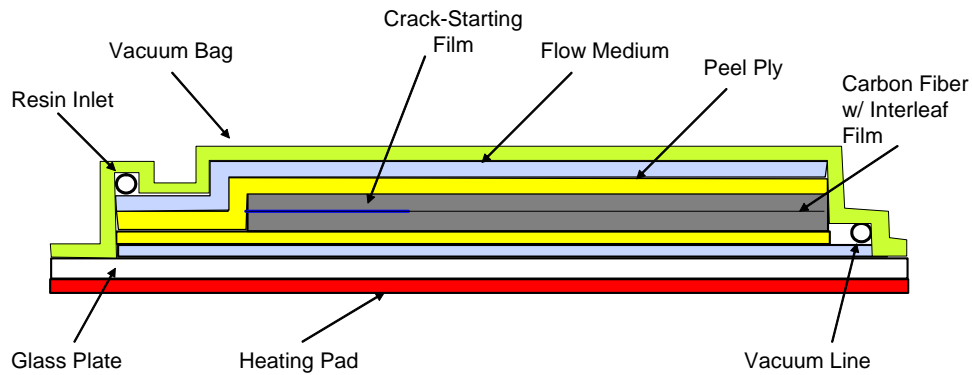


Fig. 8. Schematic of heated VARTM lay-up.

mold is brought to 65°C. After mixing, heating, and degassing of the resin/curing agent mixture, the resin reservoir is attached to the inlet tube (lower right in the figure), which is pinched closed with a clamp. The resin reservoir is maintained at 50°C during the infusion process. The outlet tube, to which the vacuum pump is attached, is then pinched closed to prevent direct application of vacuum to the resin during infusion (which can cause bubbling of the resin). The inlet tube clamp is then opened and adjusted to achieve a flow of resin into the lay-up of approximately 6mm per minute. Once the flow front of the resin has reached the end of the lay-up, the resin inlet tube and outer vacuum bag line are pinched shut with clamps. The resin reservoir and vacuum lines are then removed, and the lay-up is transferred to an oven at 122°C. The outer bag vacuum line is then reattached to the vacuum pump. The panel is then cured for two hours at 122°C, after a 15 minute heat up time, and then for two hours at 177°C, after another 15 minute heat-up time. Once the cure schedule is complete, the oven is turned off and the lay-up is allowed to cool down in the oven overnight while the vacuum is maintained on the outer bag.

## B. Experimental Procedure

Specimen dimensions and the test parameters were in compliance with ASTM Test Method D 5528 [43]. The DCB fracture specimens were  $170\text{mm}$  long and  $25\text{mm}$  wide. Hinged aluminum loading tabs (cut from piano hinge) were bonded to the outer faces of the specimens at the cracked end using an epoxy paste adhesive, placing the loading point nominally  $25\text{mm}$  from the end of the specimen and giving a nominal initial crack length of approximately  $51\text{mm}$ . The edges of the specimen were painted with a white spray enamel primer to improve the visibility of the crack tip. To provide a means of measuring the crack length, a scale printed on a self-adhesive label was applied to the painted edge of the specimen. The prepared specimen is shown in Fig. 9. After the specimen was loaded into the test frame grips, the position of the scale zero point was measured using a video camcorder mounted on a translatable stage. During the test, the crack advancement was videotaped. In this way, the crack length prior to each instance of crack growth could be measured by replaying the videotape. The timing of the video and data collection were easily correlated.

The specimen were loaded on a  $100\text{kN}$  capacity MTS<sup>©</sup> servo-hydraulic load frame in displacement control at a rate of  $3.0\text{mm}/\text{min}$ . The specimens were unloaded after the initial crack advancement, and also after the second crack advancement. This procedure would help to ensure that fracture toughness data was obtained starting at the end of the film if the initial observed crack growth was not actually from the end of the film. In most cases, the second measured toughness value would be from the first “sharp” crack, with minimal fiber bridging.

Data reduction to obtain  $G_{Ic}$ , the critical strain energy release rate, or fracture toughness, is based on the empirical compliance method proposed by Berry [44], and

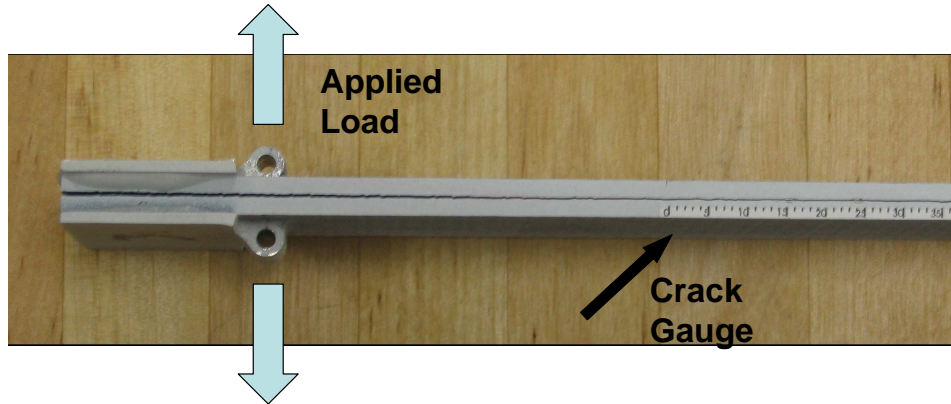


Fig. 9. DCB specimen after testing.

suggested in ASTM D 5528. The beam compliance,  $C = \delta/P$  is expressed as

$$C = \frac{a^n}{H} \quad (3.1)$$

where  $a$  is the crack length, and  $n$  and  $H$  are experimentally determined parameters.

For an ideal beam,

$$n = 3 \quad (3.2)$$

$$H = \frac{Ewt^3}{64} \quad (3.3)$$

Compliance,  $C$ , for each crack length, is calculated using the critical load,  $P_c$ , and the corresponding critical displacement,  $\delta_c$ . The critical load and critical displacement are defined as the load and displacement associated with the propagation of the crack, respectively. The exponent  $n$ , in equation 3.1, is determined from the slope the plot of  $\log C$  versus  $\log a$ . The fracture toughness,  $G_{Ic}$ , at each crack length,  $a$ , is

$$G_{Ic} = \frac{nP_c\delta_c}{2wa} \quad (3.4)$$

where  $w$  is the specimen width.

### C. Results

A minimum of four specimens each from the standard, neat, as-received and amino-functionalized XD CNT film panels were tested. Fig. 10 shows the typical load-displacement ( $P$ - $\delta$ ) curves for each panel type tested. Initial response for all specimens was linear indicating elastic loading followed by a small but sudden decrease in load. Visible cracking was also observed simultaneously with the decrease in load. In all specimens, an increase in load was then observed after which larger sudden decreases in load occurred throughout the remainder of the tests. This saw-toothed response is commonly observed in woven composites and is characterized by a stick-slip behavior as the crack is first arrested by the fiber microstructure until sufficient load is achieved to further propagate the crack [45–50]. Further toughening is achieved through fiber or ply bridging behind the crack tip and was seen throughout the specimens tested. This crack bridging mechanism serves to further accentuate the unstable, large drops in load demonstrated in the saw-tooth nature of the  $P$ - $\delta$  curves. The initial small load decrease observed at the initial crack is indicative of the initial crack propagating from the crack starter film within the matrix up to the fiber microstructure where it is arrested.

Because of the unstable nature of the crack growth within the woven composites, interlaminar fracture toughness was calculated based on the maximum load achieved just prior to each sudden load drop.  $G_{Ic}$  vs.  $a$  curves ( $R$ -curves) for all panels are shown in Fig. 11.  $G_{Ic}$  generally increased over the initial  $5mm$  before reaching a plateau region. This behavior is due to the effect of fibers bridging the crack as it grows, acting to support more load. The large amount of scatter in the data is typical of a woven fabric composite, and is attributable to the variation in microstructure due to the fabric weave as the crack tip advances as well as the effect of fiber/ply



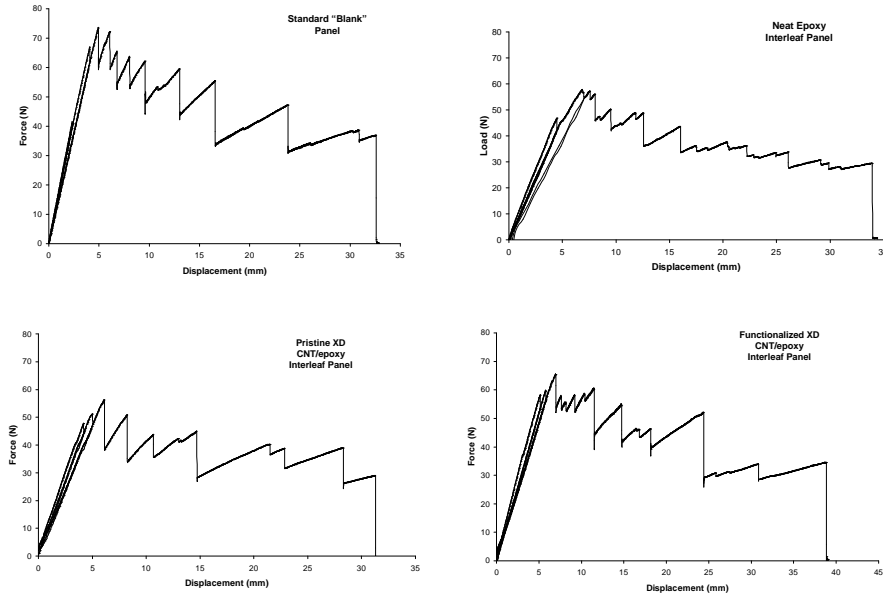


Fig. 10. Representative load-displacement curves for DCB specimens.

bridging [47].

Table V shows the average  $G_{IC}$  initiation values for all specimens tested. The average initiation value for the standard panels was calculated as  $249 J/m^2$  with a coefficient of variation ( $CoV$ ) of 29%. This agrees well with results of similar materials seen in other studies [46]. The large variation in initiation values is also not uncommon and has been attributed by Martin to the variation of placement of the crack starter insert with respect to fiber yarns [46, 47, 50]. The average initiation value for the neat epoxy interleaved panel was calculated as  $216 J/m^2$  with a  $CoV$  of 7%, a 13% reduction with respect to the non-interleaved panels. The average initiation value for the as-received XD CNT/epoxy interleaved panel was  $230 J/m^2$  with a  $CoV$  of 12%. This indicated a decrease in initiation fracture toughness of 8% for the as-received XD CNT panel with respect to the non-interleaved panels. The amino-functionalized XD CNT/epoxy interleaved panels produced the highest initiation fracture toughness

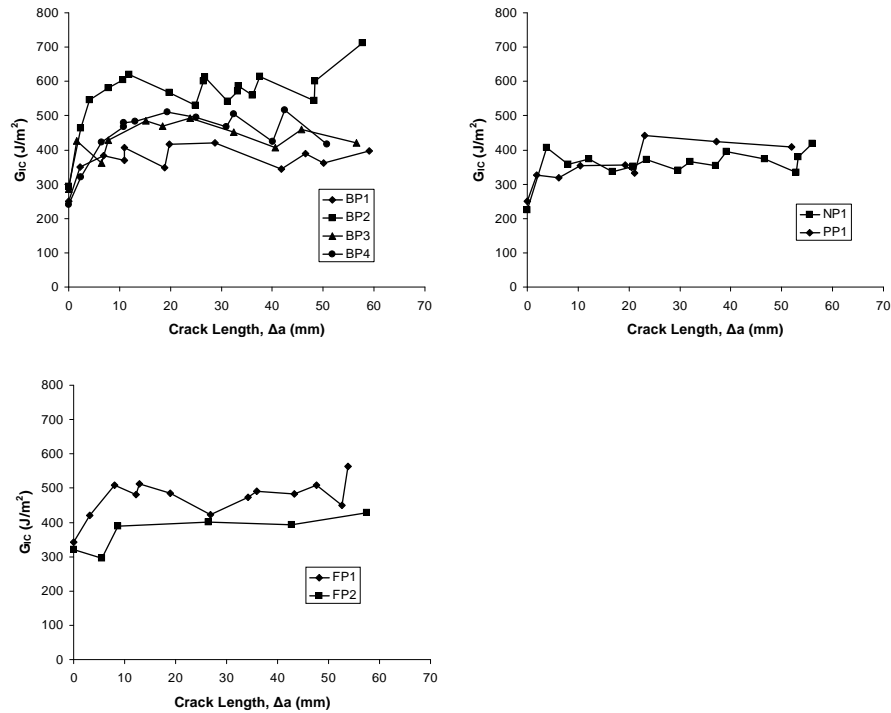


Fig. 11. Representative  $R$ -curves for DCB specimens: (a) Standard panels; (b) Neat and As-received XD CNT panels; (c) Amino-functionalized XD CNT panels.

with an average value of  $293 J/m^2$  and a  $CoV$  of 16%. This demonstrates an increase in initiation fracture toughness of 18% over non-interleaved panels and an increase of 36% over the neat epoxy interleaved panel.

Although the neat epoxy interleaved panel demonstrated a lower average initiation fracture toughness than the standard panels, t-test analysis of the data indicated that the neat film panel results were not statistically distinguishable from the standard panels. Similarly, there were no statistically significant differences between the standard panels and the as-received XD CNT/epoxy interleaved panel. This indicates that the toughness associated with the neat and as-received CNT interleaved panels are essentially the same as that observed with the standard non-interleaved

Table V. Initiation fracture toughness values.

Interleaf Type	Initiation $G_{Ic}$ ( $J/m^2$ )		
	Mean	Std. Dev.	CoV (%)
Standard Panel	248	71	29
Neat Epoxy	216	15	7
As-Received XD CNT/Epoxy	230	27	12
Functionalized XD CNT/Epoxy	293	48	16

panels. Sun et al. [41] demonstrated no increase of fracture toughness ( $K_{Ic}$ ) for 1.0 weight percent as-received XD CNT/epoxy nanocomposites compared to neat EPIKOTE 862/W. They also demonstrated an increase of 18% in  $K_{Ic}$  values for PAMAM-0 functionalized XD CNT/epoxy nanocomposites as well as an increase of 34% for PAMAM-0/epoxy specimens. This correlates well with the 18 – 36% increase in  $G_{Ic}$  of the functionalized panels with respect to the standard and neat interleaved panels observed in this study. However, the improved toughness of the PAMAM functionalized CNTs as well as the PAMAM modified epoxy shown by Sun et al. indicates that it is the addition of the dendrimer to the polymer which creates an increased fracture toughness and not the presence of the CNTs.

Table VI shows the average  $G_{Ic}$  plateau propagation values for all the panels. The average propagation for the standard panels was calculated as  $459J/m^2$  with a  $CoV$  of 22%. The average propagation for the neat epoxy interleaved panel was calculated as  $375J/m^2$  with a  $CoV$  of 9%, a 18% reduction with respect to the non-interleaved panels. The average propagation value for the as-received XD CNT/epoxy interleaved panel was  $380J/m^2$  with a  $CoV$  of 20%, a decrease in initiation fracture toughness of 17% relative to the non-interleaved panels. The amino-functionalized XD CNT produced the highest propagation fracture toughness of the interleaved panels with

an average value of  $438 J/m^2$  and a  $CoV$  of 21%. This demonstrates a decrease in propagation fracture toughness of 5% with respect to non-interleaved panels and an increase of 17% over the neat epoxy interleaved panel.

Table VI. Propagation fracture toughness values.

Interleaf Type	Propagation $G_{Ic}$ ( $J/m^2$ )		
	Mean	Std. Dev.	CoV (%)
Standard Panel	459	100	22
Neat Epoxy	375	35	9
As-Received XD CNT/Epoxy	380	76	20
Functionalized XD CNT/Epoxy	438	93	21

While the propagation fracture toughness for the standard and functionalized XD CNT/epoxy interleaved panels remained roughly equal, on average, there is a slight decrease in the propagation toughness for both the neat epoxy and as-received XD CNT/epoxy interleaved panels. This difference is due to a combination of both the type of failure as well as the amount of fiber bridging present within each specimen seen in Fig. 12.

Cohesive failure, or failure within the matrix, is evident within both the as-received and the second functionalized *FP2* panels. Additionally, there is little observed fiber bridging within the as-received panel and almost no fiber bridging observed within *FP2*. As the crack propagates, it tends to progress through the resin rich area between the fiber plies. As such, the failure is mainly Mode I and the composite toughness is entirely dependent on the local matrix toughness which the crack is propagating through. As seen in both the initiation fracture toughness results as well as in [41], the as-received XD CNT/epoxy interleave film demonstrated a fracture toughness roughly equal to that of the un-toughened bulk resin. This result,

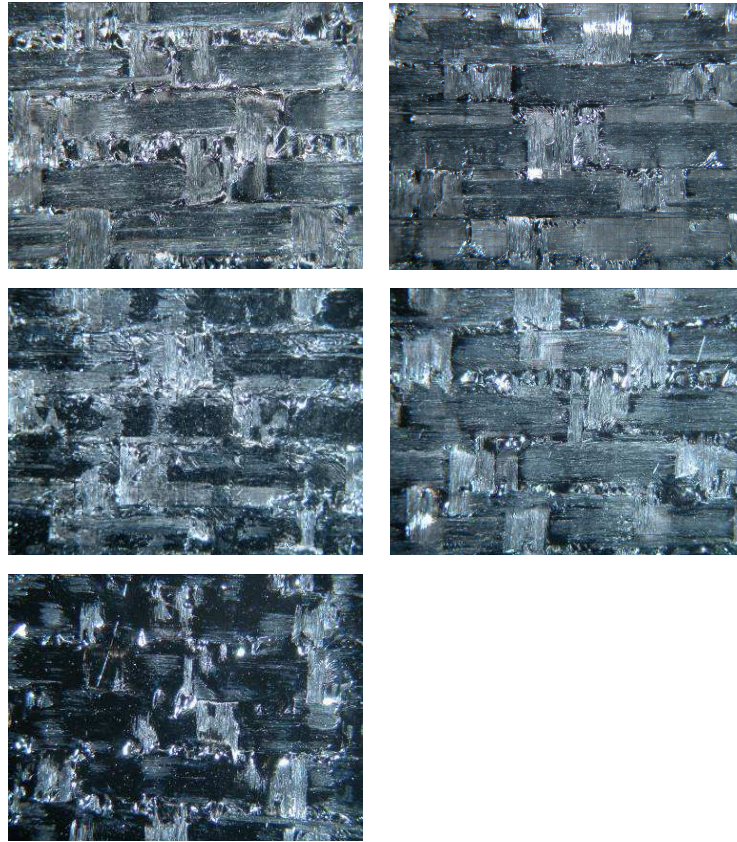


Fig. 12. Representative failure surfaces for various panels: a) Standard panels; b) Neat epoxy interleaved panel; c) As-received XD CNT/epoxy interleaved panel; d) Amino-functionalized XD CNT/epoxy interleaved panel 1; e) Amino-functionalized XD CNT/epoxy interleaved panel 2.

along with the limited amount of fiber bridging, explain the low propagation fracture toughness of the as-received interleaved panel. Fig. 13 demonstrates the difference in propagation toughness values between the first and second functionalized panels (*FP1* and *FP2*, respectively). *FP2* under-performs *FP1* by 25%. This is explained by the lack of fiber bridging within the panel. Although the *FP2* showed little, if any bridging, the toughness roughly equalled the as-received panel toughness. This is most likely due to the improved fracture toughness associated with the functionalized

film.

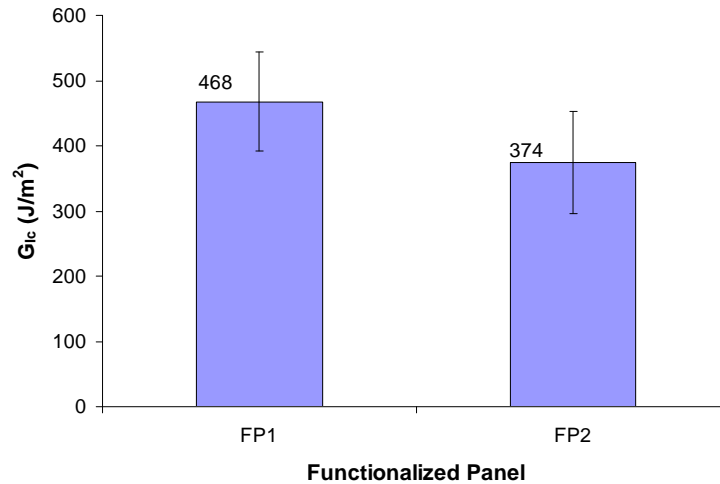


Fig. 13. Propagation fracture toughness values for functionalized panels 1 & 2.

Adhesive failure is the most commonly seen failure method within the tested panels and is associated with the propagation of the crack along the fiber/matrix interface. As the crack progresses along the fiber microstructure, it deviates more in its path, producing a mixed-mode (Mode I/Mode II) component of failure and thus increasing the observed Mode I toughness. However, just as in the case of cohesive failure, fiber bridging acts as the main toughening agent within the panels. All standard panels demonstrated significant fiber bridging along with nearly complete adhesive failure. Both the neat and *FP1* panels demonstrated adhesive failure with less fiber bridging. The presence of the films therefore reduce fiber bridging and its beneficial toughening effects. The difference between the propagation toughness values for the neat and functionalized panels is therefore indicative of the film toughness since fiber bridging is not present.

#### D. Conclusions

The effect of XD CNT modified epoxy interleaf films on the Mode I interlaminar fracture toughness of woven fabric carbon fiber/epoxy composites was examined and compared to results obtained for non-interleaved standard panels as well as panels modified with neat epoxy interleaf films. The initiation fracture toughness of panels containing the neat epoxy as well as as-received XD CNT interleaf films showed no statistically significant difference with respect to the non-interleaved standard panels. Amino-functionalized XD CNT/epoxy interleaved panels demonstrated an average 18% increase in  $G_{Ic}$  over standard panels as well as a 36% increase over the neat epoxy interleaved panel. This is most likely due to the toughening effect produced by the presence of PAMAM-0 dendrimer within the epoxy, and not a direct consequence of the presence of CNTs. The propagation fracture toughness of the functionalized XD CNT/epoxy interleaved panels was not sufficiently different than the standard panels while the neat and as-received XD CNT/epoxy interleaved panels decreased by 18% and 17% compared to the standard panels, respectively. This decrease in propagation toughness is attributed to both a suppression of fiber bridging and the inherently toughness of the interleaf films.

## CHAPTER IV

### OVERALL CONCLUSIONS AND FUTURE WORK

Carbon fiber reinforced polymer composites have a proven history as an effective structural material. However, due to a combination of both the constituent material properties as well as the physical arrangement of the constituent materials within a fiber reinforced composite, there exist areas which can limit the performance of the composite. These limitations are usually in the out-of-plane direction, especially interfacial strength, interlaminar fracture toughness, and thermal and electrical conductivity. In an effort to produce better materials, researchers have looked at ways to utilize the same material for multiple effects. This includes the use of structural materials for thermal or electrical applications such as lightning strike dissipation, electro-magnetic shielding, damage sensing and improved thermal dissipation. This multifunctionality of a material would allow for reduced weight and complexity within a system and would also possibly reduce cost as well.

Carbon nanotubes, with their small size, high electrical and thermal conductivity, and exceptional mechanical properties, are ideal candidates for producing or improving multifunctional capabilities within standard composite materials. However, due to their high cost and difficulties in dispersion, use of CNTs within the composite should be as efficient as possible. To this end, novel processing and incorporation techniques should be used to control both placement and orientation of CNTs within the bulk material. In the previous chapters, two methods of nanotube placement were investigated along with the effect these methods had on the interfacial strength and interlaminar fracture toughness of carbon fiber reinforced epoxy composites. Chemical vapor deposition proved to be a useful technique for controlling the location and orientation of multi-walled carbon nanotubes on carbon fiber



substrates. This process results in a fiber with nanotubes directly attached to the fiber surface, producing an interphase region with a large volume fraction of carbon nanotubes and potentially creating a stiff and highly conductive network transverse to the fiber length. In addition, the presence of the nanotubes increased the interfacial shear strength of the fiber by up to 71% over unsized fiber, thus improving the overall efficiency of the composite. Amine functionalized MWCNTs dispersed within a thin epoxy interleaf film provided an easily integrated method for placing CNTs within standard composite laminates. In addition to allowing for direct placement control of CNTs within a composite, these CNT-modified films were able to improve the initiation interlaminar fracture toughness by 18%. This provides not only a viable method of producing multifunctional materials, it also provides an improvement to one of the most significant limitations of standard composite laminates; interlaminar fracture toughness.

The improvements seen in the interfacial strength of MWCNT coated carbon fibers could also offer an improvement to the interlaminar fracture toughness of MWCNT/epoxy interleaved composite laminates. It was demonstrated within this study that the MWCNT-modified laminates produced an improved initiation fracture toughness due to the addition of nanotubes to the epoxy mid-layer. With the initiation fracture toughness being dominated by the inherent toughness of the matrix, the toughening effect of the nanotubes was able to have a significant effect on this property. However, once the crack began to propagate, most of the interlaminar fracture moved strictly from within the matrix to become dominated by adhesive failure along the fiber-matrix interface. Improvement in toughness associated with adhesive failure should result by strengthening the interface between fibers and matrix. Within the interfacial shear strength tests, it was shown that the presence of randomly oriented MWCNTs along a fiber improved the interfacial shear strength by 71% over unsized

fibers. Additionally, it was shown that the presence of radially aligned MWCNTs along the fiber improved the interfacial shear strength by 11%. The difference between these two values was determined to be due to the presence of nanotubes aligned along the loading direction. For the randomly oriented MWCNT coated fibers, there existed a certain percentage of nanotubes which were oriented along the shear loading direction. These tubes were able to sustain the applied load in shear and therefore enabled a strengthening effect. The radially aligned MWCNT coated fibers however, had nanotubes generally aligned perpendicular to the loading direction. These radially aligned tubes could not take the shearing load and therefore did not produce the enhancements seen within the randomly oriented specimens. Assuming that the interfacial failure due to shear can be considered representative of a Mode II failure, and observing the benefits demonstrated by the presence of nanotubes oriented along this loading direction, it is conceivable that similar results would be obtained for MWCNT coated fibers subjected to Mode I fracture, especially when the nanotubes are aligned radially. In this case, both the randomly oriented MWCNT coated fibers, with some nanotubes being aligned in the radial direction, and to a greater degree the radially aligned MWCNT coated fibers, should produce an enhanced fracture toughness when subjected to Mode I adhesive failure. The incorporation of CVD grown MWCNTs on carbon fabric plies and MWCNT/epoxy interleaf films within the same composite laminate therefore has the potential to achieve improvements in both adhesive and cohesive interlaminar fracture toughness as well as improved load transfer efficiency within the composite. By combining these mechanical improvements with the benefits associated with the high thermal and electrical conductivity of nanotubes, a multifunctional composite laminate is possible. It is therefore suggested that future effort be applied to incorporating both nanotube placement techniques within carbon fabric/epoxy composite laminates.

## REFERENCES

- [1] J. Kong, N. Franklin, C. Zhou, M. Chapline, S. Peng, K. Cho, H. Dai, Nanotube molecular wires as chemical sensors, *Science* 287 (2000) 622–625.
- [2] E. Snow, F. Perkins, E. Houser, S. Badescu, T. Reinecke, Chemical detection with a single-walled carbon nanotube capacitor, *Science* 307 (2005) 1942–1945.
- [3] S. Peng, J. O’Keeffe, C. Wei, K. Cho, J. Kong, R. Chen, N. Franklin, H. Dai, Carbon nanotube chemical and mechanical sensors, in: *Proc. 3rd Int. Workshop on Structural Health Monitoring*, 2001, pp. 1–8.
- [4] I. Kanga, Y. Heunga, J. Kimb, J. Leed, R. Gollapudia, S. Subramaniamc, S. Narasimhadevaraa, D. Hurda, G. Kirikeraa, V. Shanovc, M. Schulza, D. Shic, J. Boerioc, S. Malle, M. Ruggles-Wrene, Introduction to carbon nanotube and nanofiber smart materials, *Composites Part B* 37 (2006) 382–394.
- [5] K. Loh, J. Kim, J. Lynch, N. Wong Shi Kam, N. Kotov, Multifunctional layer-by-layer carbon nanotube-polyelectrolyte thin films for strain and corrosion sensing, *Smart Mater Struct* 16 (2007) 429–438.
- [6] E. Thostenson, T. Chou, Carbon nanotube networks: sensing of distributed strain and damage for life prediction and self healing, *Adv Mater* 18 (2006) 2837–2841.
- [7] R. Baughman, C. Cui, A. Zakhidov, Z. Iqbal, J. Barisci, G. Spinks, G. Wallace, A. Mazzoldi, D. De Rossi, A. Rinzler, O. Jaschinski, S. Roth, M. Kertesz, Carbon nanotube actuators, *Science* 284 (1999) 1340–1344.

- [8] M. Biercuk, M. Llaguno, M. Radosavljevic, J. Hyun, J. Fischer, A. Johnson, Carbon nanotube composites for thermal management, *Appl Phys Lett* 80 (2002) 2767–2869.
- [9] H. Huang, C. Liu, Y. Wu, S. Fan, Aligned carbon nanotube composite films for thermal management, *Adv Mater* 17 (2005) 1652–1656.
- [10] V. Veedu, A. Cao, X. Li, K. Ma, C. Soldano, S. Kar, P. Ajayan, M. Ghasemi-Nejhad, Multifunctional composites using reinforced laminae with carbon-nanotube forests, *Nat Mater* 5 (2006) 457–462.
- [11] Q. Zhang, J. Liu, R. Sager, L. Dai, J. Baur, Carbon nanotubes on carbon fibers: influence of growth conditions on fiber tensile properties, in: *SAMPE Fall Technical Conference and Exhibition*, SAMPE, 2007.
- [12] E. Thostenson, C. Li, T. Chou, Nanocomposites in context, *Compos Sci Technol* 65 (2005) 491–516.
- [13] R. Baughman, A. Zakhidov, W. de Heer, Carbon nanotubes- the route toward applications, *Science* 297 (2002) 787–792.
- [14] L. Dai, A. Patil, X. Gong, Z. Guo, L. Liu, Y. Liu, D. Zhu, Aligned nanotubes, *ChemPhysChem* 4 (2003) 1150–1169.
- [15] L. Drzal, M. Rich, P. Lloyd, Adhesion of graphite fibers to epoxy matrices: I. the role of fiber surface treatment, *J Adhes* 16 (1982) 1–30.
- [16] L. Drzal, M. Rich, M. Koenig, P. Lloyd, Adhesion of graphite fibers to epoxy matrices: II. the effect of fiber finish, *J Adhes* 16 (1983) 133–152.
- [17] B. Agarwal, R. Bansal, Effect of an interfacial layer on the properties of fibrous composites: a theoretical analysis, *Fibre Sci Technol* 12 (1979) 149–158.

- [18] E. Thostenson, W. Li, D. Wang, Z. Ren, T. Chou, Carbon nanotube/carbon fiber hybrid multiscale composites, *J Appl Phys* 91 (2002) 6034–6037.
- [19] Y. Xu, L. Cheng, L. Zhang, H. Yin, X. Yin, C. You, Effects of chemical vapor infiltration atmosphere on the mechanical properties and microstructure of carbon fibers, *J Eur Ceram Soc* 21 (2001) 809–816.
- [20] A. Kelly, W. Tyson, Tensile properties of fibre-reinforced metals: copper/tungsten and copper/molybdenum, *J Mech Phys Solids* 13 (1965) 329–350.
- [21] A. Netravali, R. Henstenburg, S. Phoenix, P. Schwartz, Interfacial shear strength studies using the single-filament-composite test: I. experiments on graphite fibers in epoxy, *Polym Compos* 10 (1989) 226–241.
- [22] T. Skourlis, R. McCullough, The effect of temperature on the behavior of the interphase in polymeric composites, *Compos Sci Technol* 49 (1993) 363–368.
- [23] J. Nairn, S. Harper, W. Bascom, Effects of fiber, matrix, and interphase on carbon fiber composite compression strength, Contractor Report 4601, NASA (1994).
- [24] D. Tripathi, F. Jones, Single fibre fragmentation test for assessing adhesion in fibre reinforced composites, *J Mater Sci* 33 (1998) 1–16.
- [25] F. Zhao, T. Okabe, N. Takeda, Effect of matrix yield properties on fragmentation behavior of single fiber composites, *Compos Interfaces* 9 (2002) 289–308.
- [26] B. Kim, J. Nairn, Observations of fiber fracture and interfacial debonding phenomena using the fragmentation test in single fiber composites, *J Compos Mater* 36 (2002) 1825–1858.

- [27] S. Feih, K. Wonsyld, D. Minzari, P. Westermann, H. Lilholt, Testing procedure for the single fiber fragmentation test, Tech. Rep. Risø-R-1483(EN), RisøNational Laboratory (2004).
- [28] T. Ohsawa, A. Nakayama, M. Miwa, A. Hasegawa, Temperature dependence of critical fiber length for glass fiber-reinforced thermosetting resins, *J Appl Polym Sci* 22 (1978) 3203–3212.
- [29] I. Beyerlein, S. Pheonix, Statistics for the strength and size effects of microcomposites with four carbon fibers in epoxy resin, *Compos Sci Technol* 56 (1996) 75–92.
- [30] L. Lee, S. Rudov-Clark, A. Mouritz, M. Bannister, I. Herszberg, Effect of weaving damage on the tensile properties of three-dimensional woven composites, *Compos Struct* 57 (2002) 405–413.
- [31] S. Deng, P. Rosso, L. Ye, K. Friedrich, Interlaminar fracture of CF/EP composites modified with nano-silica, *Solid State Phenom* 121 (2007) 1403–1406.
- [32] F. Gojny, M. Wichmann, U. Kpke, B. Fiedler, K. Schulte, Carbon nanotube-reinforced epoxy-composites: enhanced stiffness and fracture toughness at low nanotube content, *Compos Sci Technol* 64 (2004) 2363–23716.
- [33] K. Awasthi, S. Awasthi, A. Srivastava, R. Kamalakaran, S. Talapatra, P. Ajayan, O. Srivastava, Synthesis and characterization of carbon nanotube-polyethylene oxide composites, *Nanotechnology* 17 (2006) 5417–5422.
- [34] F. Gojny, K. Schulte, Functionalisation effect on the thermo mechanical behaviour of multi-wall carbon nanotube/epoxy-composites, *Compos Sci Technol* 64 (2004) 2303–2308.

- [35] F. Gojiny, J. Nastalczyk, R. Zbiginew, K. Schulte, Surface modified multi-walled carbon nanotubes in CNT/epoxy-composites, *Chem Phys Lett* 370 (2003) 820–824.
- [36] O. Ishai, H. Rosenthal, N. Sela, E. Drukker, Effect of selective adhesive interleaving on interlaminar fracture toughness of graphite/epoxy composite laminates, *Composites* 19 (1988) 49–54.
- [37] A. Xuefeng, J. Shuangying, T. Bangming, Z. Zilong, Y. Xiao-Su, Toughness improvement of carbon laminates by periodic interleaving thin thermoplastic films, *J Mater Sci Lett* 21 (2002) 1763–1765.
- [38] S. Singh, I. Partridge, Mixed-mode fracture in an interleaved carbon-fiber/epoxy composite, *Compos Sci Technol* 55 (1995) 319–327.
- [39] Product Data Sheet HS-CP-5000, Hexcel Composites, Stamford, Connecticut (2007).
- [40] Product Data Sheet SC:1183-02, Resolution Performance Products LLC, Houston, Texas (2002).
- [41] L. Sun, G. Warren, J. O'Reilly, W. Everett, S. Lee, D. Davis, D. Lagoudas, H. Sue, Mechanical properties of surface-functionalized SWCNT/epoxy composites, doi:10.1016/j.carbon.2007.11.051 (2008).
- [42] R. Bolick, A. Kelkar, Innovative composite processing by using H-VARTM method, presented at SAMPE 2007 Technical Conference, Paris, France (April 2007).
- [43] ASTM International, Standard test method for mode I interlaminar fracture

- toughness of unidirectional fiber-reinforced polymer matrix composites, in: D 5528-01, West Conshohocken, Pennsylvania, 2001.
- [44] J. Berry, Determination of fracture surface energies by the cleavage technique, *J Appl Phys* 34 (1963) 62–68.
- [45] A. Mouritz, C. Bains, I. Herszberg, Mode I interlaminar fracture toughness properties of advanced textile fiberglass composites, *Composites Part A* 30 (1999) 859–870.
- [46] I. Paris, P. Minguet, T. O’Brien, Comparison of delamination characterization for IM7/8552 composite woven and tape laminates, in: *Composite Materials: Testing and Design Fourteenth Volume*, ASTM STP 1436, West Conshohocken, Pennsylvania, 2003.
- [47] N. Alif, L. Carlsson, J. Gillespie, Mode I, mode II, and mixed mode interlaminar fracture of woven fabric carbon/epoxy, in: *Composite Materials: Testing and Design Thirteenth Volume*, ASTM STP 1242, West Conshohocken, Pennsylvania, 1997.
- [48] N. Alif, L. Carlsson, L. Boogh, The effect of weave pattern and crack propagation direction on mode I delamination resistance of woven glass and carbon composites, *Composites Part B* 29 (1998) 603–611.
- [49] P. Hansen, R. Martin, DCB, 4ENF and MMB delamination characterisation of S2/8552 and IM7/8552, Technical Report N68171-98-M-5177, Materials Engineering Research Laboratory Ltd. (MERL), Hertford, U.K. (1999).
- [50] R. Martin, Delamination characterization of woven glass/polyester composites, *J Compos Tech Res* 19 (1997) 20–28.



## VITA

Ryan Sager is married and has one son. He received his B.S. in aerospace engineering from Texas A&M University in May of 2006. He then enrolled in the graduate program in aerospace engineering at Texas A&M University in the fall of 2006, where he has worked under the guidance of Dr. Dimitris C. Lagoudas. His research interests include the material characterization of nanocomposites, as well as fabrication of fiber reinforced polymer composites. An extended resume can be found at <http://nanoags.tamu.edu>. Mr. Sager can be reached at his permanent address: 411 Mae Dr. Justin, TX, 76247. His email address is [rsager2001@yahoo.com](mailto:rsager2001@yahoo.com).